Evaluation of Water Sorption Behavior and *In Vitro* Blood Compatibility of Polyvinyl Alcohol Based Magnetic Bionanocomposites

A. K. Bajpai, Rashmi Gupta

Department of Chemistry, Bose Memorial Research Laboratory, Government Autonomous Science College, Jabalpur, Madhya Pradesh 482001, India

Received 17 October 2008; accepted 14 June 2009
DOI 10.1002/app.30953
Published online 12 August 2009 in Wiley InterScience (www.interscience.wiley.com).

ABSTRACT: In recent past magnetic bionanocomposites have shown potential in biomedical applications mainly due to their superparamagnetic and biocompatible nature. They have also established themselves as a promising class of hybrid organic–inorganic materials derived from polymers and organic/inorganic fillers. In this study biocompatible nanocomposites were prepared by *in situ* synthesis of magnetic nanoparticles within the polyvinyl alcohol-grafted-polymethyl methacrylate hydrogels and characterized by techniques such as FT-IR, scanning electron microscopy, transmission electron microscopy, X-ray diffraction, and differential scanning calorimetry. The bionanocomposites were evaluated for water sorption behavior and *in vitro* biocompatibility by performing thrombus formation and hemolysis tests. The influence of chemical composition of the grafted hydrogel was investigated on water sorption behavior and *in vitro* blood compatibility of magnetic bionanocomposites. © 2009 Wiley Periodicals, Inc. J Appl Polym Sci 114: 3548–3560, 2009

Key words: nanocomposites; polymer; hydrogel; blood compatibility; swelling

INTRODUCTION

Bionanocomposites form a fascinating interdisciplinary area that brings together biology, material science, and nanotechnology. New Bionanocomposites are impacting diverse areas, in particular biomedical science where these innovative materials have found tremendous applications. The general goal in the design and fabrication of all composites has been to combine two or more different materials to produce a single material that behaves as a homogenous entity and has predictable and reproducible properties. With appropriate design, composite combines the best qualities of each component, producing a material with properties that are superior to each component. Generally, polymer nanocomposites are the result of the combination of polymers and inorganic/organic fillers at the nanometer scale. The interaction between filler components of nanocomposites at nanodimension enables them to act as molecular bridges in the polymer matrix. This is the bases for enhanced mechanical (stiffness and toughness), thermal (flammability resistance), biological, magnetic, optical, electronic, and optoelectronic properties as compared with the corresponding inorganic or polymer component only.[1–5]

Nanostructured magnetic material are now being extensively studied for high capacity magnetic storage media, integrated circuits, color imaging, magnetic refrigerators, and used for a variety of biomedical application.[6] These applications include myocardial tissue engineering[7]; cell labeling and magnetic separation[8–10]; MRI contrast agents[11,12] hyperthermia and thermal ablation[13]; gene therapy[14] and site specific drug targeting; and controlled release technology.[15–18]

Fe_3O_4 (magnetite) is a technologically important biocompatible magnetic material that has a wide spectrum of applications ranging from cell separation and drug delivery to hyperthermia. According to Chang et al.,[19,20] *in vitro* cytotoxicity test revealed that the magnetite particles exhibited excellent biocompatibility. Below a critical size, nanocrystalline magnetic particles may be a single domain and show the unique phenomenon of superparamagnetism.[21] Superparamagnetism is an important magnetic property because it allows the nanoparticles to be magnetized under the influence of a magnetic field, but not to retain residual magnetism in its absence.[22–25]

Thus, being motivated by the significant and diversified applications of magnetic nanocomposites in this work a new method has been proposed for preparation of magnetic bionanocomposites that

Correspondence to: A. K. Bajpai (akbmrl@yahoo.co.in).

involves *in situ* synthesis of magnetic nanoparticles within a hydrogel matrix prepared by graft copolymerization of methyl methacrylate (MMA) onto polyvinyl alcohol (PVA). Hydrogels are versatile materials composed of three dimensional structures of macromolecular chains and owe unique biophysical properties such as high water content, low modulus and elasticity, softness, permeability to gases like oxygen, low frictional resistance to surrounding tissues, etc.[26] All these properties enable them to deserve as a promising candidate for biomedical and pharmaceutical applications. For this reason this study is also focused on the water sorption behavior of polyvinyl alcohol-grafted-polymethyl methacrylate (PVA-*g*-PMMA) hydrogel and evaluation of *in vitro* biocompatibility of the synthesized magnetic bionanocomposites.

Among various synthetic hydrophilic polymers used in the preparation of hydrogel, poly(vinyl alcohol) has a prime position in biomedical science, because of it's inherent nontoxicity, noncarcinogenicity, good biocompatibility, and desirable properties such as a rubbery or elastic nature and a high degree of swelling in aqueous solution. PVA hydrogels have gained wide biomedical applications in articular cartilage replacement, as a pharmaceutical release agent, reconstructive surgery, drug delivery, etc.[27]

Polymethyl methacrylate (PMMA) has been selected as another component for polymer-inorganic composites because it has superior intrinsic physio-chemical properties like higher softening point and higher tensile strength as well as myriad of uniqueness including optical clarity, biocompatibility, and dimensional stability. PMMA has also been employed as a popular material for various technological and biomedical applications.[28,29] Some of its biomedical applications include bone cement[30] and cell labeling.[31] PMMA has been widely employed in targeted drug delivery systems, in which the polymer encapsulated drugs are provided protection from biomolecules inside the body before reaching the target site.[32]

EXPERIMENTAL

Materials

PVA (98% hydrolyzed, soluble in hot water at 80°C, mol wt ca. 14,000), was obtained from E. Merck, India, and used without any pretreatment. Monomer, MMA was obtained from Sigma Aldrich Co. and washed thrice in 5% NaOH, 5% H_2SO_4, and bidistilled water, respectively and freed from the inhibitor by distilling it under vacuum. *N*, *N*'-methylenebisacrylamide (MBA) (Research Lab Mumbai, India) was used as a crosslinking agent while potassium persulphate (Loba Chemie, India) and potassium metabisulphite (Qualigens Fine Chemicals, Mumbai, India) were used as initiator and activator, respectively. $FeCl_2{\cdot}4H_2O$ and $FeCl_3{\cdot}6H_2O$ salts were obtained from Merck (India) and used as received. Bidistilled water was used throughout the experiments.

Methods

Preparation of iron oxide nanoparticles

For synthesis of iron oxide nanoparticles the solution of Fe ions was prepared from $FeCl_2{\cdot}4H_2O$ and $FeCl_3{\cdot}6H_2O$ salts ($Fe^{2+}/Fe^{3+} = 0.5$) in acidic condition by continuous stirring the solution for 0.5 h under nitrogen atmosphere and at room temperature as per the modified method reported in literature.[33,34] A solution of NH_4OH/NaOH was added dropwise into the solution of Fe ions to precipitate nanoparticles of iron oxide according to the reaction given below:

$$2FeCl_3 + FeCl_2 + 8NH_4OH \rightarrow Fe_3O_4 + 8NH_4C1 + 4H_2O$$

The precipitated iron oxide nanoparticles were filtered and repeatedly washed with distilled water. The washed and dried nanoparticles were stored in air tight containers.

Preparation of grafted hydrogel

The hydrogel was prepared by a redox polymerization method as reported in earlier publication.[35] In brief, known amounts of PVA, purified monomer MMA and crosslinker (MBA) were taken in aqueous medium and precalculated amounts of redox system comprising of persulphate and metabisulphite were added into the reaction mixture in one shot to initiate graft copolymerization. The reaction mixture was taken in a rectangular glass mould (8 cm × 10 cm) and kept for 24 h at 35°C so that the whole fluid converted into a semitransparent thin film. The thickness of the gel was found to be 0.048 cm for PVA variation, 0.047 cm for MMA variation and 0.053 cm for MBA variation, respectively. The scheme of graft copolymerization may be described as below:

$$S_2O_5^{2-} + H_2O \rightarrow 2HSO_3^-$$

$$HSO_3^- \rightarrow H^+SO_3^{2-}$$

$$SO_3^{2-} + S_2O_8^{2-} \rightarrow SO_4^{2-} + SO_{R^*}^{\bullet 4-} + SO_{R^*}^{\bullet 3}$$

TABLE I
Data Showing the Kinetic Parameters for the Water Sorption Process

S. No	PVA/MMA wt (g)% ratio	MBA (mmol)	Penetration velocity ($V \times 10^5$ cm/sec)	Diffusion constant ($D \times 10^8$ cm^2/sec)	n	Mechanism
1	0.71	0.06	0.91	7.1	0.62	Anomalous
2	1.07	0.06	0.93	7.9	0.58	Anomalous
3	1.60	0.06	0.70	6.8	0.71	Anomalous
4	2.13	0.06	1.16	7.7	0.63	Anomalous
5	2.67	0.06	1.20	8.3	0.65	Anomalous
6	3.2	0.06	1.10	7.4	0.78	Anomalous
7	4.28	0.06	1.42	8.2	0.56.	Anomalous
8	2.13	0.00	1.39	10.3	0.75	Anomalous
9	2.13	0.19	0.59	6.7	0.64	Anomalous
10	2.13	0.26	0.37	6.0	0.63	Anomalous

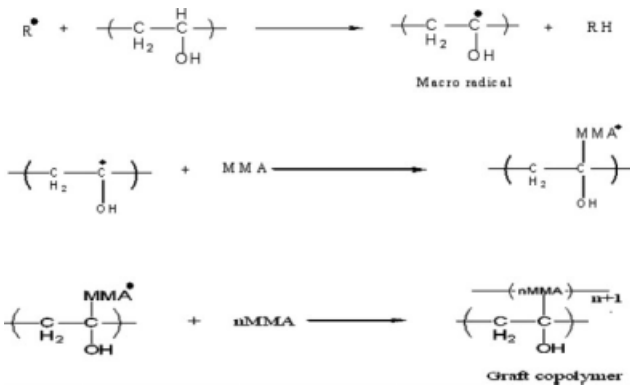

Purification of hydrogel

The thin film prepared as above was allowed to swell in bidistilled water till equilibrium so that the unreacted chemicals including salts leached out, and the gel becomes free of any unreacted impurities. The fully swollen gel was dried at room temperature, and the film was cut into small rectangular pieces (1 cm × 1 cm) and stored in airtight polyethylene bags.

Swelling experiments

The extent of swelling of grafted hydrogel was determined by a conventional gravimetric procedure as reported in literature.[36] In a typical experiment, preweighed pieces of hydrogel (without iron oxide) were allowed to swell in distilled water for 24 h (up to equilibrium swelling). Thereafter, the pieces were taken out from the water and gently pressed in-between the two filter papers to remove excess of water and finally weighed using a sensitive balance (APX–203 Denver, Germany). The swelling ratio was determined by the following eq. (1),

$$\text{Swelling ratio}(S_r) = \frac{\text{Weight of swollen gel}}{\text{Weight of dry gel}} = \frac{(W_s)}{(W_d)} \quad (1)$$

The amount of water imbibed by the sample provides information about the hydrophilic nature of the material, which is essentially a criterion for biocompatibility.

To determine the nature of the mechanism of transport of water molecules within the gel and evaluate their diffusion coefficient, the following equations were used[37]:

$$\frac{W_t}{W_\infty} = k\, t^n \quad (2)$$

$$\frac{W_t}{W\infty} = 4\left(\frac{D\, t}{\pi\, L^2}\right)^{0.5} \quad (3)$$

where W_t and W_∞ are the water intakes at time t and at equilibrium, respectively, k is the swelling rate front factor, n is the swelling exponent, D is the diffusion constant and L is the thickness of the dry gel. The values have been calculated for various compositions of the gel and are summarized in Table I.

Penetration velocity measurements

The penetration velocity for each composition was determined by the weight-gain method as described by Peppas and Franson.[38] The values of penetration velocities were calculated from the slope of the initial portion of the penetrant uptake curve using the following eq. (4);

$$V = \left(\frac{dW_g}{dt}\right) \times \left(\frac{1}{\rho}\right) \times \left(\frac{1}{2A}\right) \quad (4)$$

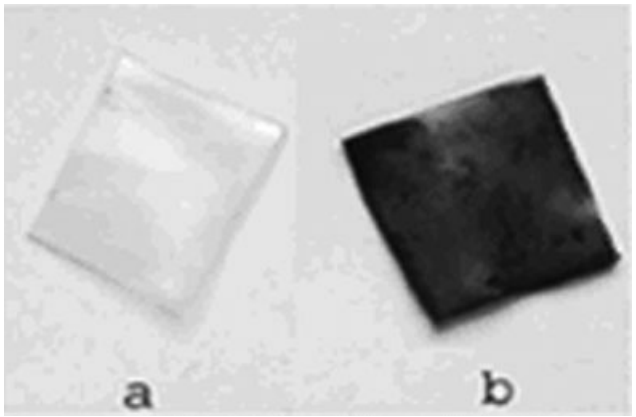

Figure 1 Physical appearance of (a) PVA-*g*-PMMA hydrogel and (b) iron oxide impregnated PVA-*g*-PMMA hydrogel of definite composition: [PVA/MMA (wt %) = 2.13] [MBA] = 0.06 m*M*.

where V is the penetration velocity, dW_g/dt is slope of the weight-gain versus time curve p the density of water, A is the area of one face of the disc, and the factor 2 accounts for the fact that penetration takes place through both the faces. The penetration velocities calculated for various compositions of hydrogels are summarized in Table I.

Impregnation of ion oxide into the gel

The dried and purified gels were placed in an equimolar aqueous solution of mixture of ferrous (0.5 M) and ferric salts (0.6 M) and allowed to swell for 24 h so that both ferrous and ferric ions were entrapped into the polymer matrices. Before putting them in salt solutions a dry stream of N_2 was flushed for at least 1 h. The swollen gels were taken out and washed by mildly shaking them in distill water so that surface of gel was properly washed and freed from unreacted salts and chemicals. It is worth mentioning here that as the gel is already swollen, the possibility of expulsion of salts from the gel may be ruled out. The gel was dried at room temperature for 72 h and dried gels were then put into alkaline solution (10% NaOH or NH_4OH) for 24 h so that ferrous and ferric ions get precipitated within the polymer matrix and formation of magnetite is obtained. The formation of magnetite is confirmed by the change in color of the gel which turns from red to dark red-brown. Figure 1(a,b), depict physical appearance of the native grafted and iron oxide impregnated hydrogels which also confirm the formation of iron oxides within the polymer gel matrix. As evident from the photographs, the native hydrogel is white and semitransparent in color, whereas the impregnated hydrogel appears dark red brown in color, which could be attributed to the formation of iron oxide within the matrix. The prepared iron oxide-polymer nanocomposites were washed, dried at room temperature for a week, and stored in airtight polyethylene bags.

The percentage impregnation of iron oxide into the gel was calculated by the following eq. (5):

$$[\%]\ \text{Impregnation of iron oxide} = \frac{\{W_{\text{impregnated}} - W_{\text{dry}}\}}{W_{\text{dry}}} \times 100 \quad (5)$$

where $W_{\text{impregnated}}$ is the weight of dry impregnated gel and W_{dry} is the initial weight of hydrogel.

Characterization of nanocomposites

The prepared nanocomposites were characterized by the following methods as discussed below.

FT-IR. To provide an evidence for grafting of PMMA chains onto PVA backbone and impregnation of magnetite into the grafted hydrogel matrix, FTIR spectra of native PVA and iron oxide impregnated hydrogels were recorded from 4000 to 400 cm^{-1} using an FTIR-8400S, Shimadzu spectrophotometer. The prepared films were directly mounted on spectrophotometer.

Electron microscopy study. The morphological features of the nanocomposites and iron oxide particles were investigated by recording scanning electron micrographs (STEREO SCAN, 430, Lecica, SEM) of the nanocomposites and transmission electron micrographs (Hitachi Hu-11 B) of the iron oxide particles.

X-ray diffraction. The X-ray diffraction studies of the nanocomposites were carried out on Rigaku Rotting anode mode Ru-H3R (18 KW), X-ray powder diffractometer. The diffraction data were collected from 10 to 70°, 2° θ values with a step size of 0.02° and counting time of 2 s $step^{-1}$ using a wavelength of 1.54 Å. The average crystallite size of iron oxide particles were estimated using Scherrer's formula.

Differential scanning calorimetry. The thermal properties of the nanocomposites were studied by constructing their differential scanning thermograms on a TA instrument DSC-2C (Perkins–Elmer, Inc.) under inert atmosphere taking nitrogen as purging gas. The experiments were performed from room temperature to 400°C at a heating rate of 10°C/min. The sample weights were in the range of 7–10 mg.

Magnetization studies using VSM. Vibrating sample magnetometer (Oxford, VSM) was used to evaluate magnetic moments of both the prepared iron oxide nanoparticles and nanocomposites at room temperature as a function of the applied magnetic field.

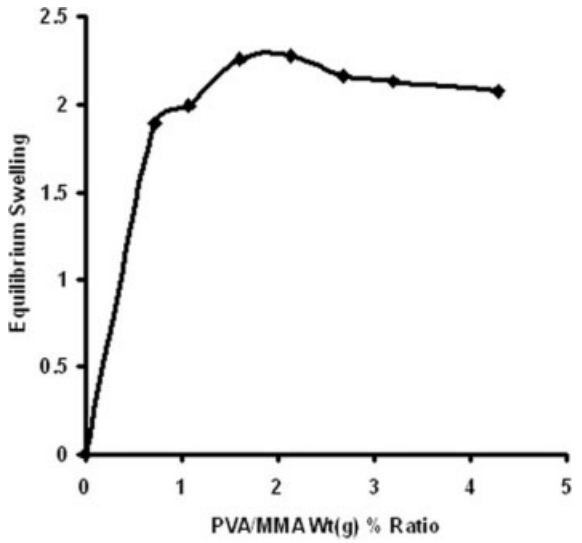

Figure 2 Effect of PVA/MMA wt % Ratio on the equilibrium swelling ratio of the hydrogel of definite composition: [MBA] = 0.06 m*M*.

Blood compatibility studies

The *in vitro* blood compatibility of the prepared nanocomposites was determined by the methods described as below:

Thrombus formation tests. The antithrombogenicity of the composite surface was judged by the blood-thrombus formation test, as described elsewhere.[39] In brief, the specimens were equilibrated with saline water (0.9% w/v NaCl) at 37°C for 24 h. in a constant temperature bath. To these swollen samples was added ACD blood (0.5 mL) followed by the addition of $CaCl_2$ solution (0.03 mL of 4 mol L^{-1}**)** to start the thrombus formation. Adding of deionized water (4.0 mL) stopped the reaction and the thrombus formed was separated by soaking in water for 10 min at room temperature and then fixed in 36% formaldehyde solution (2.0 mL) for another 10 min. The fixed thrombus was removed with the help of a brush by gently scratching the clot from the hydrogel surface. The removed thrombus was placed in water for 10 min and, after drying, its weight was recorded. The same procedures were repeated for glass surface, blood bags, and the composites of varying compositions and respective weights of thrombus formed were recorded.

% Haemolysis tests. Haemolysis experiments were performed on the surfaces of prepared gels as described elsewhere.[39] In a typical experiment, a dry composite piece (4 cm^2) was equilibrated in normal saline water (0.9% w/v NaCl) at 37°C for 24 h and human ACD blood (0.25 mL) was added into the gels. After 20 min, 2.0 mL of 0.9% sodium chloride (saline water), was added to each sample to stop haemolysis, and the samples were incubated at 37°C for 60 min. Positive and negative controls were obtained by adding 0.25 mL of human ACD blood and 0.9% NaCl solution, respectively to 2.0 mL of bidistilled water. Incubated samples were centrifuged for 45 min, the supernatant was taken, and its absorbance was recorded on a spectrophotometer (Systronics Model No. 106, India) at 545 nm. The percentage haemolysis was calculated using the following relationship:

$$(\%)\ \text{Hacmolysis} = \frac{A_{\text{test-sample}} - A_{(-)\text{control}}}{A_{(+)\text{control}} - A_{(-)\text{control}}} \times 100 \quad (6)$$

where A is absorbance. The absorbance of positive and negative controls was found to be 1.26 and 0.004, respectively.

RESULTS AND DISCUSSION

Water sorption studies

Effect of PVA/MMA ratio

Among various structural factors influencing water sorption capacity of a polymer hydrogel, the ratio of hydrophilicity to hydrophobicity plays a key role in determining swelling characteristics of the hydrogel matrix. In this study, the prepared matrix is composed mainly of PVA and PMMA, which are known hydrophilic and hydrophobic polymers, respectively, and their relative amounts in the gel are expected to affect extent of swelling of the hydrogels significantly. To study the impact of hydrophilicity/hydrophobicity ratio on water sorption capacity of the hydrogel the weight % ratio (g/g) was varied in the range 0.71–4.28 and equilibrium water sorption (i.e., swelling ratio after 24 h) was recorded. The results are shown in Figure 2 which clearly reveals that the equilibrium swelling ratio increases with increasing % weight ratio from 0.71 to 2.13, whereas beyond it a fall in equilibrium swelling was noticed. The observed results may be explained as below:

Since PVA is a hydrophilic polymer its increasing weight % in the gel in the range 0.71–2.13 results in an enhanced hydrophilicity of the matrix, which leads to more and more sorption of water. In a similar way the decreasing wt % of MMA, a hydrophilic component, in the hydrogel will also result in greater swelling of the hydrogel.

The decrease observed, however, beyond wt % 2.13 of PVA may be explained by the fact that with much greater increase in wt % of PVA its chains are held to one another via hydrogen bonds of their OH groups and may result in a more crosslinked and compact structure of the hydrogel through meshes of which the penetration of water molecules gets restrained and, as a consequence, the equilibrium swelling decreases. It is also likely that due to

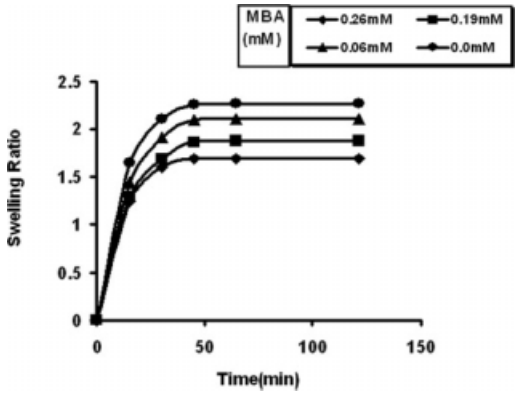

Figure 3 Effect of varying amounts of MBA on the swelling ratio of the hydrogel of definite composition: [PVA/MMA (wt %) = 2.13].

hydrogen bonding the chains of PVA lose their mobility results in a fact in the water sorption capacity of the gel. Similar types of results have also been reported elsewhere.[40]

Effect of MBA

The effect of crosslinker on the degree of water sorption has been investigated by employing different amounts of cross linking agent (MBA) in the range 0.00–0.26 m*M*. The results are shown in Figure 3 which clearly reveal that the swelling ratio constantly decreases with increasing crosslinker concentration. The observed fall in swelling ratio is quite obvious because with increasing crosslinker concentration the crosslink density increases to an appreciable extent and does not favor penetration of water molecules into the network and, therefore, the swelling of hydrogel decreases.

It is notable here that although the hydrogel without crosslinker shows optimum swelling ratio, however, it does not dissolve during swelling which was further confirmed by monitoring the weights of dry hydrogels after repeating several swelling–deswelling cycles. The aquatic stability of the hydrogel may be attributed to the fact that hydrophobic PMMA chains grafted onto PVA molecules render it almost insoluble in aqueous media. Some authors[41] have reported an increase in the T_g of the polymer with increasing concentration of crosslinker. This also results in a restrained mobility of network chains and therefore, slows down the swelling.

Effect of pH

In this investigation the effect of pH has been investigated in the range 1.4–11.2, and the results are depicted in Figure 4. It is clear from the Figure that the equilibrium swelling increases with increasing pH of the swelling medium and attains an optimum

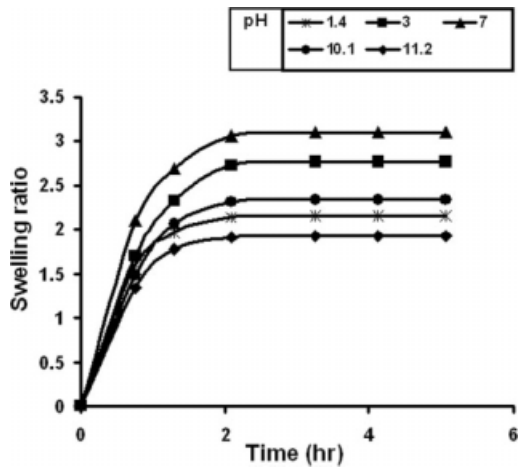

Figure 4 Effect of pH on the swelling ratio of the hydrogel of definite composition: [PVA/MMA (wt %) = 2.13], [MBA] = 0.06 m*M*.

swelling at neutral pH. However, after increasing the pH in alkaline range the swelling ratio decreases. The results may be explained as below:

According to Flory's theory of swelling of network[42] apart from other structural factors degree of swelling is also determined by the concentration difference of ions present inside (C_i^g) and outside (C_i^s) the network. This difference results in an ion osmotic pressure ($\prod$ion) given by the following equation.

$$\prod \text{ion} = RT \sum (C_i^g - C_i^s) \tag{7}$$

It is clear from the above equation that larger the difference in concentration, greater would be the osmotic pressure and, therefore, the swelling ratio. In this work, however, since the hydrogel is nonionic in nature, the swelling will be dependent on the

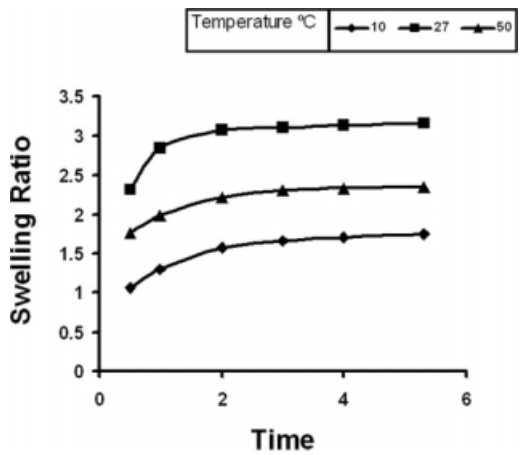

Figure 5 Effect of temperature on the swelling ratio of the hydrogel of definite composition: [PVA/MMA (wt %) = 2.13], [MBA] = 0.06 m*M*.

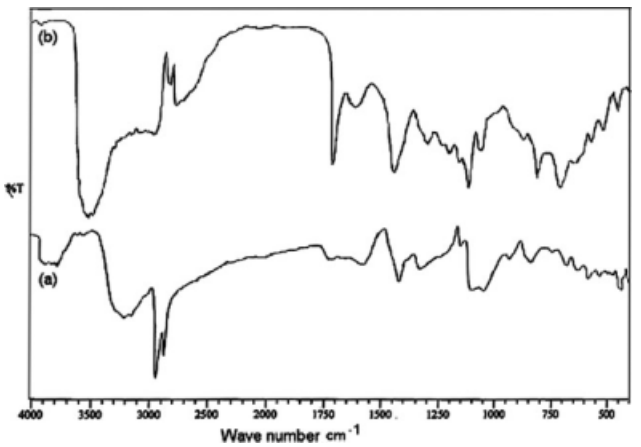

Figure 6 FTIR spectra of (a) native PVA (b) iron oxide impregnated gel of definite composition: [PVA/MMA (wt %) = 2.13], [MBA] = 0.06 m*M*.

concentration of ions (C_i^s) outside the solution. Thus, greater the value of C_i^s, smaller will be the swelling of the hydrogel.

In this work when the pH is 1.4, the concentration of H^+ and CI^- ions is quite large and, therefore, ∏ion will be small and swelling will be low. However, when the pH is raised from 1.4 to 7.4 by addition of NaOH, the concentration of H^+ ions decreases and as a consequence, the swelling increases up to optimum at neutral pH. However, beyond pH 7.0, when the pH is raised further in alkaline range by addition of NaOH, the concentration of OH^- and Na^+ ions increases which again lower the swelling ratio to a minimum.

Effect of temperature

In this study, the effect of temperature on the degree of water sorption has been investigated by carrying out water sorption experiments in the range 10–50°C. The change in temperature of swelling medium controls the diffusion of water molecules into the gel, segmental mobility of the network chains, and water-polymer interactions. The results are presented in Figure 5 which reveals that the swelling ratio initially increases up to 27°C, whereas beyond it, a decrease is observed. Thus, a maximum swelling is attained at 27°C. The observed results may be explained by the fact that on increasing temperature the mobility of macromolecular chains of the network also increases, which permits greater number of water molecules to enter into the network. However, there is a decrease in swelling ratio with increases temperature beyond 27°C, and this may be due to the breaking of the hydrogen bonds between the water molecules and network chains.

FTIR spectra

The FTIR spectra of native PVA and prepared iron oxide impregnated hydrogels of a definite composition are depicted in Figure 6(a,b), respectively .The spectra (b) clearly reveals that the iron oxide impregnated gel presents combined spectral features of various functional groups of PVA and PMMA. Moreover, some characteristic bonds of iron oxide are also present.

Figure 6(b), represents the FTIR spectra of iron oxide impregnated PVA-*g*-PMMA gel film, as evident from the peaks observed at 3487 and 3526 cm^{-1} (typical of hydrogen bonded (bridged) O—H

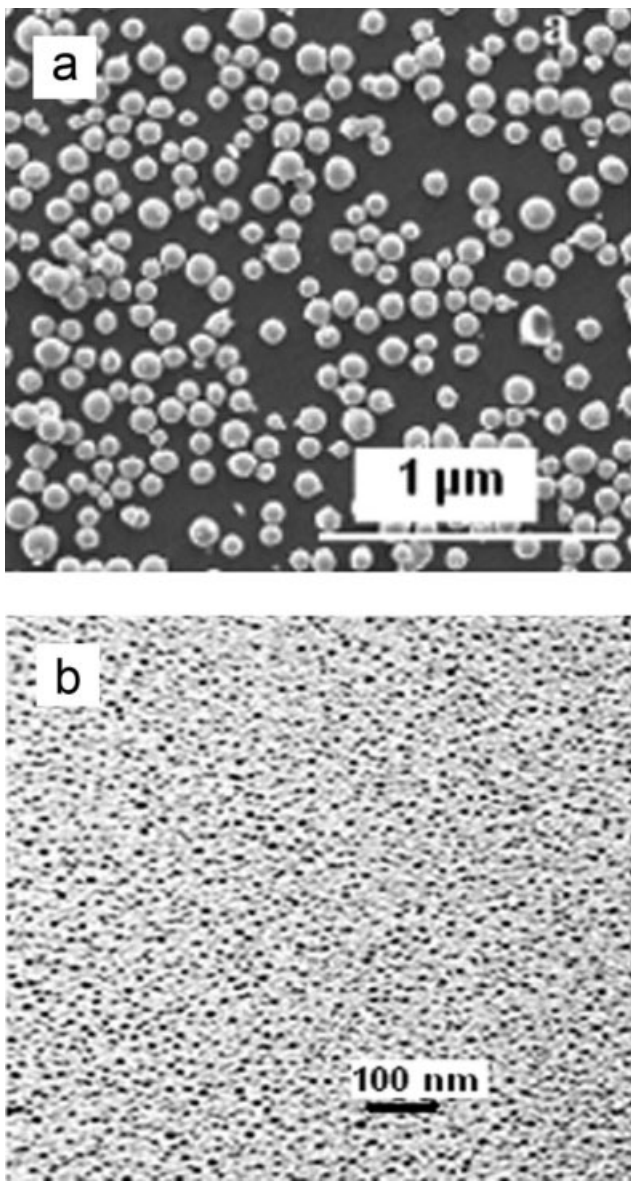

Figure 7 SEM image of (a) iron oxide impregnated gel of definite composition: [PVA/MMA (wt %) = 2.13], [MBA] = 0.06 m*M* and (b) TEM image of iron oxide nanoparticles.

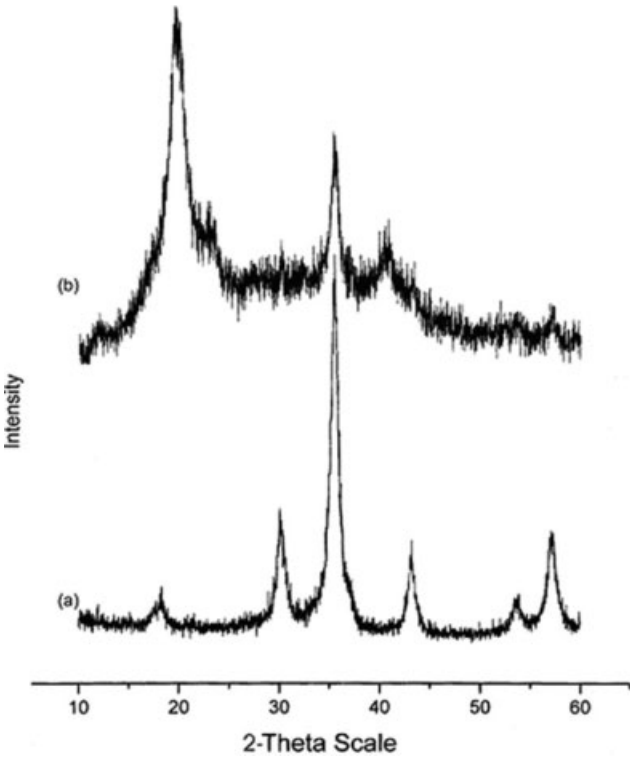

Figure 8 XRD spectra of (a) iron oxide nanoparticles and (b) iron oxide impregnated gel of definite composition: [PVA/MMA (wt %) = 2.13], [MBA] = 0.06 m*M*.

stretching vibrations of alcoholic OH and bound water), 2999 cm^{-1} (from C—H stretching of CH, CH_2, and CH_3 groups), 1157 and 1342 cm^{-1} (from twisting and wagging vibrations of methylene group, 1479 cm^{-1} (due to SP^3 C—H bending) 1111 cm^{-1} (due to C—O stretching of alcohol).

The characteristic peaks in Figure 6(b), appearing at 1741 cm^{-1}, 1654 cm^{-1}, and 1214 cm^{-1} indicate the presence of stretching vibrations of the C=O ester group , C=C group and asymmetric coupled vibrations of C—C(=O)—O group of PMMA respectively, which also confirm the grafting of PMMA onto PVA.

The presence of iron oxide in the hydrogel is evident from the absorption bands appeared in the region between 450 and 480 cm^{-1}, and they may be assigned to Fe-O bonds of magnetite.[43] The peaks at 521, 761, and 862 cm^{-1} may also be due to the iron oxide lattice deformation[44] and OH groups bound to the surface of the Fe_3O_4 nanoparticles. The spectra also show a peak at 581 cm^{-1}, characteristic of magnetite,[45] and thus indicate the presence of magnetite particles in the polymer matrix.

Electron microscopy

The morphological features of the prepared impregnated gels have been investigated by SEM and transmission electron microscopy (TEM) analysis of iron oxide particles are shown in Figure 7(a,b), respectively.

Scanning electron microscopy

A close examination of the micrograph of iron oxide impregnated polymer matrix in Figure 7(a), shows a homogeneous and even surface morphology. The impregnated iron oxide particles exhibit uniform size of nanometer dimensions.

Transmission electron microscopy

To examine size of the iron oxide particles at nanoscale level TEM studies were performed. The TEM image shown in Figure 7(b), reveals that an average size of the nanoparticles are about 9.52 nm and shape of the particles is also uniform.

X- ray diffraction

To study the crystallographic nature of iron oxide nanoparticles and nanocomposite the XRD analysis was performed and XRD spectra are shown in Figure 8(a,b), respectively. The spectral patterns for iron oxide particles shown in Figure 8(a), indicate the characteristic peaks at 18.2°, 30.0°, 35.4°, 43.1°, 53.3°, 57.0°. The interplaner distances using Bragg's equation were calculated to be 4.875, 2.979, 2.536, 2.099, 1.719, and 1.615 Å, respectively. The well defined x-ray diffraction patterns indicate the formation of highly crystalline iron oxide nanoparticles. The results also indicate that the prepared nanoparticles

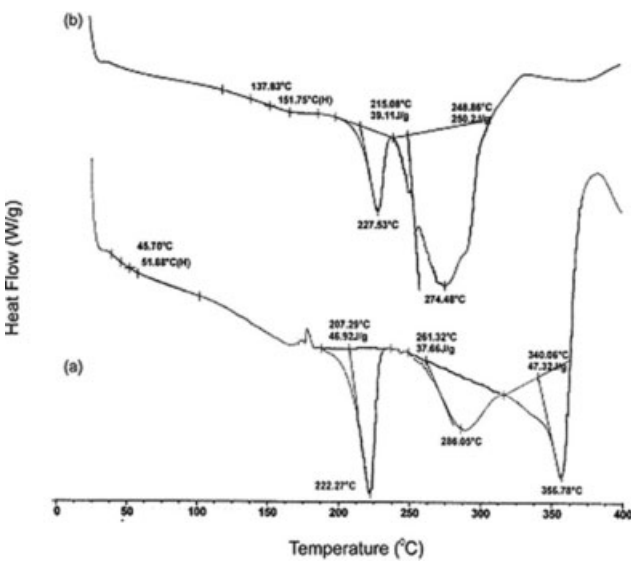

Figure 9 DSC thermograms of (a) native (PVA-*g*-MMA) gel and (b) iron oxide impregnated gel of definite composition: [PVA/MMA (wt %) = 2.13], [MBA] = 0.06 m*M*.

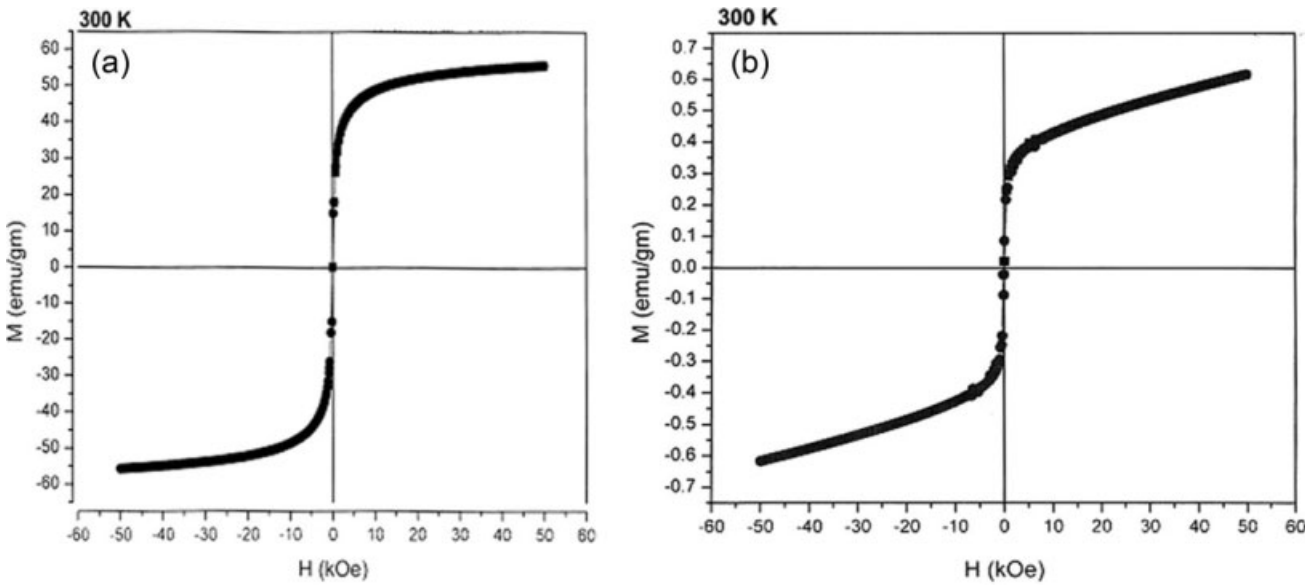

Figure 10 Magnetization versus applied field curves (a) and (b) for magnetic nanoparticles and magnetic nanocomposites at 300 K of definite composition: [PVA/MMA (wt %) = 2.13], [MBA] = 0.06 m*M*.

are pure magnetite with an inverse cubic spinal structure, which are identical to the standard XRD patterns of Fe_3O_4.[46] X-ray diffraction patterns of the nanocomposite film shown in Figure 8(b), indicate the characteristic peaks for poly(vinyl alcohol) and iron oxide at a 2θ values of 19.5 and 35.4 with their interplanner distances 4.554 and 2.536 Å, respectively. PVA is known to be of semicrystalline nature and shows a single broad peak at 19.5Å. The XRD spectra shown in Figure 8(b), depict an extra peak at 35.4°, thus, suggesting for characteristic peak of iron oxide. This obviously indicates the formation of iron oxide (magnetite) within the polymer matrix.

It is also clear from the Figure 8(a,b), that the spectral intensity of the diffraction peaks of iron oxide in the composite is smaller as compared with that of the bulk nanoparticles due to the concentration of nanoparticles is much smaller in the composite.

The mean grain size was calculated using Debye-Scherrer formula[47] as shown in eq. (8):

$$d = \frac{K\lambda}{\beta \cos \theta} \tag{8}$$

where d is mean grain size, k is the shape factor (0.9), β is broadening of the diffraction angle and λ is diffraction wavelength (1.54 Å).

From, XRD spectra the crystallite size of iron oxide nanoparticles has been estimated to be 8.3 nm, which is in close agreement with the value of 9.52 nm calculated from TEM image.

Differential scanning calorimetry

PVA is known to be a semicrystalline polymer in which high physical interaction between the polymer chains arise due to hydrogen bonding between the hydroxyl groups.[48] The interaction of another polymer with PVA either as a grafted chain or through a crosslinker significantly alters the thermal properties of the native polymer.[49] The thermograms of native and iron oxide impregnated gels are depicted in Figure 9(a,b), respectively which may be explained as below:

The curve 9 (a) shows a very minor transition at onset temperature 46.7°C which could be assigned to glass temperature (T_g) of PVA. The obtained value is lower than the reported values of 85°C for 98–99% hydrolyzed PVA and 58°C for 87–89% hydrolyzed PVA[50] and may be attributed to the reason that the bulky PMMA chains could be grafted onto PVA backbone molecules, thus enhancing their flexibility. This obviously results in a fall in the T_g of PVA based matrix. The curve 9 (a) shows a major endotherm at 222°C which may be attributed to melting of pendent groups of PVA chains. A high enthalpy of 46.9 J/g represents highly crystalline nature of the matrix. The Figure 9(a), also shows two major endotherm at 286 and 356°C, which may be assigned to degradation of PVA and PMMA chains, respectively.

The impregnation of iron oxide seems to have brought a significant change in thermal behavior of the gel as evident from the thermogram shown in Figure 9(b).It is clear from the curve that a minor endotherm is obtained at 137°C, which could

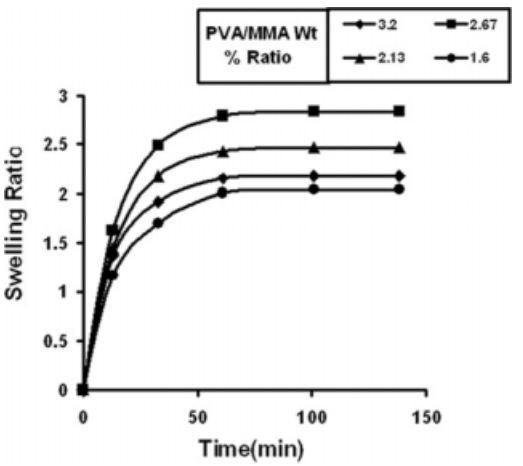

Figure 11 Effect of varying amounts of PVA on the swelling ratio of the hydrogel of definite composition: [MBA] = 0 .06 m*M*.

probably be due to the glass transition temperature of PVA. The obtained T_g of PVA is quite higher than the reported values and may be explained by the fact that incorporation of iron oxide nanoparticles into the polymer matrix enhances the rigidity of macromolecular chains which in turn increases the value of T_g. The thermograms also depict an endotherm at 227°C, which represents melting of pendent groups of PVA. Another much prominent endotherm with significantly higher value of enthalpy of 250 J/g is seen at 274°C and may be attributed to the melting of backbone of PVA. The large peak area represents highly crystalline nature of the nanocomposite, which is obviously due to the impregnation of iron oxide nanoparticles into the matrix. It is to be noted in the thermograms that no glass transition appears for PMMA up to 400°C, and this may be explained by the fact that inclusion of iron oxide particles might have increased the rigidity of PMMA chains which, therefore, may undergoes transition at much higher temperature.

Magnetization studies

Magnetic properties of a nanocomposite material are of great significance as their magnitude eventually determines the nature of application where the composite material has to be used in. Thus, realizing the need to explore the nature of magnetic behavior of the prepared nanocomposites, variation in magnetic moments of prepared iron oxide nanoparticles, and their polymer composites was investigated as a function of varying magnetic field in the range—60–60 kOe. The results are shown in Figure 10(a,b), which represent M-H plots for bulk nanoparticles (a) and nanocomposites (b), respectively.

Figure 10(a), shows a typical magnetization (M) versus the applied magnetic field (H) plot. The saturation magnetization of the synthetic magnetic particles was found to be equal to 55 emu/g at 300 K. The values obtained are lower than the reported values of 92–100 emu/g for magnetite (Fe_3O_4) nanoparticles[51] and may be attributed to the fact that below a critical size, nanocrystalline magnetic particles may be a single domain and show the unique phenomenon of superparamagnetism.[52] The reason for this behavior may be that thermal effects, although not strong enough to overcome the forces between individual atoms, are strong enough to change the magnetization direction of the entire particle, which results in a random arrangement of magnetic directions among crystallites, thus giving a magnetic moment of zero.

Similar type of results is found when magnetite-polymer nanocomposites are investigated for M-H studies. The magnetization curves were constructed by measuring the magnetic moment with increasingly applied magnetic field varying in the range −60 to 60 kOe as shown in Figure 10(b). The results clearly reveal that saturation magnetization is not attained even up to 60 kOe. The plot, however, indicates a zero remnant magnetization and coercivity thus suggesting the superparamagnetic behavior of nanocomposites. The magnetization values, however, are significantly lower values, which is quite obvious also as diamagnetic nature of polymer matrix lowers the magnetization values. It is worth mentioning here that the observed remnance and zero coercivity clearly imply that *in situ* formation of magnetic nanoparticles within the polymer matrix produces much smaller sized particles which could also be a reason for lower magnetization values of the nanocomposite materials and may be attributed

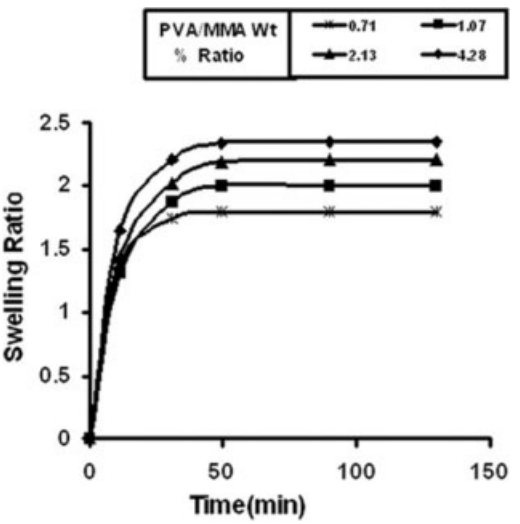

Figure 12 Effect of varying amounts of MMA on the swelling ratio of the hydrogel of definite composition: [MBA] = 0.06 m*M*.

TABLE II
Data Showing the Effect of Composition of the Hydrogel on *in vitro* Blood Compatibility Parameters

S. No	PVA/MMA wt (g) % ratio	MBA (mmol)	% Haemolysis	Clot formation (mg)	% Impregnation
1	0.71	0.06	49.8	3.9	5.71
2	1.07	0.06	46.7	1.5	7.14
3	1.6	0.06	35.4	1.9	10.0
4	2.13	0.06	25	1.2	11.4
5	2.67	0.06	31.5	4.7	7.14
6	3.2	0.06	52	4.9	5.71
7	4.28	0.06	54.3	6.8	5.42
8	2.13	0.00	42.6	1.0	10.0
9	2.13	0.19	45.5	1.3	7.14
10	2.13	0.26	55.5	8.5	5.71
11	Glass surface	–	32.6	30.0	–
12	PVC (blood bag)	–	13.75	1.0	–

to the fact that below a critical size, nanocrystalline magnetic particles may be single domain and show the unique phenomenon of superparamagnetism.

Analysis of kinetic sorption data

To evaluate the kinetic constants of water sorption process swelling ratio versus time plots of PVA, MMA, and MBA (Figs. 11, 12, and 3) were utilized and values of n, D, and V were calculated in accordance with the eqs. (2), (3), and (4), respectively. The calculated kinetic constants have been summarized in Table I.

The phenomenon of water sorption mechanistically depends on the diffusion of water molecules into the polymer matrix and subsequent relaxation of macromolecular chains of the three dimensional network. These two dynamic processes determine nature of the water transport mechanism whether the swelling process is fickian or nonfickian. It is clear from the data presented in Table I that variation in the composition of the hydrogel does not significantly affect the value of n. In all the cases, the swelling exponent n is found in the nonfickian region thus suggesting an anomalous water transport process. The observed results could be attributed to the fact that because of the grafting of PMMA chains onto the PVA, the macromolecular matrix results in a loose structure with wide pores and adequate chain flexibility. Thus, the relative rates of diffusion of water molecules and network chains relaxation become almost identical and this gives rise to an anomalous ($R_{diff} \sim R_{relax}$) type of water sorption mechanism.

Blood compatibility studies

The prepared iron oxide-polymer nanocomposites have been investigated for *in vitro* blood compatibility by carrying out blood clot formation and present haemolysis tests as described in the experimental section. The results are summarized in Table II which shows the influence of chemical composition of the nanocomposites on blood compatibility parameters. The results may be discussed as below:

When the weight % ratio (w/w) of PVA/MMA varies in the matrix from 0.71 to 4.28 an optimum antithrombogenity is noticed for 2.13 wt. ratio whereas for nanocomposites with lower and higher amounts of PVA content, both the amount of blood clot and percent haemolysis are quite higher. The reason for the observed results could be that for lower (0.71 and 1.07) and higher (2.67 and 3.2) wt % ratio of PVA, both the polymer components, i.e., hydrophilic PVA and hydrophobic PMMA may not be fully physically compatible to produce a homogenous matrix. Thus, due to chemical inhomogeniety of the nanocomposite its surface may not respond favorably to contacting blood and relatively higher amounts of blood clots and percent haemolysis are obtained.

In the case of variation of crosslinker (MBA) in the range 0.00–0.26 mM, it is found that both the % haemolysis and weight of blood clot increase significantly. The results may be attributed to the fact that being hydrophilic in nature the increasing concentration of crosslinker tends to enhance hydrophobicity of the nanocomposite which, in turn, results in increase thrombogenity as evident from the observed higher values of % haemolysis and weight of blood clot.

It is also evident from the data that the nanocomposites with greater % impregnation of iron oxide exhibit greater blood compatibility which may be due to the blood compatible nature of iron oxide.

CONCLUSIONS

Redox polymerization of MMA in the presence of PVA results in a polymer matrix of adequate

hydrophilicity and mechanical strength. The matrix functions as an ideal medium for homogenous *in situ* precipitation of magnetite nanoparticles, which is further confirmed by FTIR.

The water sorption property of a native hydrogel is greatly determined by the chemical composition of the matrix. When % wt ratio of PVA/MMA increases in the range 0.71–4.28, the swelling ratio increases up to 2.13 while thereafter a fall is noticed. However, with increasing crosslinker MBA (up to 0.26 m*M*) the extent of water sorption constantly decreases. The degree of water sorption also varies with varying pH and temperature of the swelling bath. It is found that as neutral pH (7.0) and moderate temperature (27°C) the swelling becomes optimum. The water sorption process also follows non-fickian type transport mechanism.

The SEM suggests that the surface of the iron oxide impregnated polymer matrix has a homogeneous and even morphology. The nanocomposite contains magnetite particles having nanolevel dimension. The TEM of the nanoparticles suggests for an average size of 9.52 nm of the magnetite nanoparticles.

The XRD analysis of bulk magnetite nanoparticles and nanocomposite reveal that the former are more crystalline in nature and their incorporation into the polymer matrix brings about a fall in the overall crystallinity. The size of the nanoparticles calculated by Debye-Scherrer equation has been found to be 8.3 nm, which agrees very well with that estimated by TEM.

The DSC measurements of both the native and the iron oxide-impregnated hydrogels indicate that inclusion of magnetite particles into the polymer matrix results in an enhanced crystallinity as evident from large enthalpy change (250 J/g) accompanying melting of polymer matrix.

When the prepared iron oxide nanoparticles and nanocomposites are put under varying magnetic field, magnetic moment is developed that increases with increasing field strength. It is also observed that the magnetic moment of bulk nanoparticles is much greater than nanocomposite matrices, and both the bulk nanoparticles and nanocomposites exhibit superparamagnetic behavior.

The *in vitro* blood compatibility as judged by the clot formation and percent haemolysis data depend on the chemical composition of the magnetite-polymer nanocomposites. It is found that the nanocomposites matrix offers an optimum antithrombogenicity at 2.13 weight ratio of PVA/PMMA content, whereas the thrombogenicity increases with increasing content of crosslinker (MBA). The blood compatibility also increases with increasing % impregnation of iron oxide.

Thus, the prepared magnetite-polymer matrix shows superparamagnetic and biocompatible properties and may serve as potential candidate for biomedical applications.

The authors wish to acknowledge the University Grants Commission, Department of Atomic Energy (UGC-DAE) Consortium for Scientific Research, Indore, India, for the magnetization measurements, TEM and XRD analysis.

References

1. Hule, R. A.; Pochan, D. J. MRS Bull 2007, 32, 354.
2. Kelly, A., Eds. An Introduction to Composite Material in A Concise Encyclopedia of Composite Materials; Elsevier: Oxford, 1994, xvii–xxix.
3. Gerstle, F. P., Jr.; Kroschwitz, J. I.; Mark, H. F.; Bikales, N. M.; Overberger, C. G.; Menges, G., Eds. Composites in Encyclopedia of Polymer Science and Technology; Wiley: New York, 1985.
4. Ahmad, Z.; Sarwar, M. I.; Mark, J. E. Mater Chem Phys 1997, 96, 259.
5. Schmidt, H.; Schloze, H.; Tunker, G. J Non-Cryst Solids 1986, 80, 557.
6. Zhitomirsky, I.; Niewczas, M.; Cao, J. J Mater Chem Phys 2006, 96, 289.
7. Shimizu, K.; Ito, A.; Lee, J. K.; Yoshida, T.; Miwa, K.; Ishiguro, H.; Numaguchi, Y.; Murohara, T.; Kodama, I.; Honda, H. Biotechnol Bioeng 2007, 96, 803.
8. Freeman, W. J. J Integr Neurosci 2005, 4, 407.
9. Seesod, N.; Nopparat, P.; Hedrum, A.; Holder, A.; Thaithong, S.; Uhlen, M.; Lundeberg, J. Am J Trop Med Hyg 1997, 56, 322.
10. Ugelstad, J.; Stenstad, P.; Kilaas, L.; Prestvik, W. S.; Herje, R.; Berge, A.; Hornes, E. Blood Purif 1993, 11, 349.
11. Kohler, N.; Sun, C.; Wang, J.; Zhang, M.; Langmuir 2005, 21, 8858.
12. Suwa, T.; Ozawa, S.; Ueda, M.; Ando, N.; Kitajima, M.; Int J Cancer 1998, 75, 626.
13. Gu, H.; Xu, K.; Yang, Z.; Chang, C. K.; Xu, B. Chem Commun (Camb) 2005, 34, 4270.
14. Xu, H.; Song, T.; Bao, X. Q.; Hu, L. L. J Magn Magn Mater 2005, 293, 514.
15. De Paoli, V. M.; De Paoli, L. S. H.; Spinu, L.; Ingber, B.; Rosenzweig, Z.; Rosenzweig, N. Langmuir 2006, 22, 5894.
16. Rana, S.; Gallo, A.; Srivastava, R. S.; Misra, R. D. K. Acta Biomater 2007, 3, 233.
17. Yang, J.; Park, S. B.; Yoon, H. G.; Huh, Y. M.; Haam, S. Int J Pharm 2006, 324, 185.
18. Zhang, Y.; Kohler, N.; Zhang, M. Biomaterials 2002, 23, 1553.
19. Reiss, G.; Huetten, A. Nat Mater 2005, 4, 725.
20. Chang, F. Y.; Su, C. H.; Yang, Y. S.; Yeh, C. S.; Tsai, C. Y.; Wu, C. L.; Wu, M. T.; Shieh, D. B. Biomaterials 2005, 26, 729.
21. Zhitomirsky, I.; Niewczas, P. A. Mater Lett 2003, 57, 1045.
22. Kim, K. S.; Park, J. K. Lab Chip 2005, 5, 657.
23. Pankhurst, Q. A.; Connolly, J.; Jones, S. K.; Dobson, J. J Phys D Appl Phys 2003, 36, R167.
24. Safarik, I.; Safarikova, M. Monatshefte Fur Chemie 2002, 133, 737.
25. Tartaj, P.; Morales, M. D.; Veintemillas - Verdaguer, S.; Gonzalez – Carreno T.; Serna, C. J. J Phys D Appl Phys 2003, 36, R182.
26. Ramires, P. A.; Miccoli, M. A.; Panzarini, E.; Dini, L.; Protopapa, C. J Biomed Mater Res Part B: Appl Biomater 2005, 72B, 230.
27. Bajpai, A. K.; Saini, R. Polym Int 2005, 54, 796.
28. Huang, X.; Brittain, W. J. Macromolecules 2001, 34, 3255.
29. Kalogeras, I. M.; Vassilikou-Dova, A.V. J Phys Chem B 2001, 105, 7651.

30. Sivakuma, M.; Rao, K. P. J Biomater Sci Polym Ed 2002, 13, 111.
31. Nagao, D.; Anzai, N.; Kobayashi, Y.; Gu, S.; Konno, M. J Colloid Interface Sci 2006, 298, 232.
32. Owais, M.; Gupta, C. M. Curr Drug Deliv 2005, 2, 311.
33. Mockovciakova, A.; Orolinova, Z.; Matik, M.; Hudec, P.; Kmecova, E. Acta Montanistica Slovaca 2006, 11, 353.
34. Kang, Y. S.; Risbud, S.; Rabolt, J. F.; Stroeve, P. Chem Mater 1996, 8, 2209.
35. Bajpai, A. K.; Kankane, S. J Appl Polym Sci 2007, 104, 1559.
36. Bajpai, A. K.; Singh, R. Polym Int 2007, 56, 557.
37. Bajpai, A. K.; Shrivastava, M. J Macromol Sci Pure Appl Chem A 2002, 39, 667.
38. Peppas, N. A.; Franson, N. M. J Polym Sci Polym Phys 1983, 21, 983.
39. Imai, Y.; Nose, Y. J Biomed Mater Res 1972, 6, 165.
40. Bajpai, A. K.; Bajpai, J.; Shukla, S. React Funct Polym 2001, 50, 9.
41. Bajpai, A. K.; Bajpai, J.; Shukla, S. Macromol Res 2003, 11, 273.
42. Flory, P. J. Principles of Polymer Chemistry; Cornell University Press: Ithaca, New York, 1953.
43. Zhong, Z. Y.; Prozorov, T.; Felner, I.; Gedanken, A. J Phys Chem B 1999, 103, 947.
44. Kryszewski, M.; Jeszka, J. K. Synth Mater 1998, 94, 99.
45. Schwartzman, V.; Cornell, R. M. Iron Oxide in the Laboratory: Preparation and Characterization, 2nd ed.; Wiley: New York, 2000.
46. Mandal, M.; Kundu, S.; Ghosh, S. K.; Panigrahi, S.; Sahu, T. K.; Yusuf, S. M.; Pal, T. J Colloid Interface Sci 2005, 286, 187.
47. Bajpai, A. K.; Bundela, H.; Polym Lett 2008, 2, 201.
48. Hidalgo, M.; Reinecke, H.; Mijangos, C. Polymer 1999, 40, 3535.
49. Krumova, M.; Lopez, D.; Benavente, R.; Mijangos, C.; Perena, J. M. Polymer 2000, 41, 9265.
50. Finch, C. A.; Polyvinyl Alcohol–Developments; Wiley: Chichester, 1992.
51. Morales, M. A.; Jain, T. K.; Labhasetwar, V. J Appl Phys 2005, 97, 10Q905.
52. Chia, C. H.; Zakaria, S.; Ahamd, S.; Abdullah, M.; Jani, S. M. Am J Appl Sci 2006, 3, 1750.